Sensorless Metal Object Detection for Wireless Power Transfer Using Machine Learning

***Purpose*—This work aims to realize a sensorless metal object detection using machine learning, to prevent the wireless power transfer system from the risks of electric discharge and fire accidents caused by foreign metal objects.**

***methodology*— The data constructed by analyzing the input impedance using finite element method are used in machine learning. From the loci of the input impedance of systems, the trained neural network, support vector machine, and naive Bayes classifier judge if a metal object exists. Then the proposed method is tested by experiments too.**

***Findings*— In the test using simulated data, all of the three machine learning methods show high accuracy over 80% for detecting an aluminum cylinder. And in the experimental verifications, the existence of an aluminum cylinder and empty can are successfully identified by neural network.**

***Value*— This work provides a new sensorless metal object detection method for wireless power transfer using three machine learning methods. And it shows that neural network obtain high accuracy than the others in both simulated and experimental verifications.**

***Index Terms*—machine learning, metal object detection, wireless power transfer.**

I. INTRODUCTION

For recent decades, the attention to electric vehicles (EV) has been increasing because of the environmental concerns relevant to air pollution and global warming. This has stimulated the research and development of wireless power transfer (WPT) providing a safer and more reliable charging solution for EV. Until now, many studies focusing on the design of the transmission and receiving coils, including the classical circular [1] and double D patterns which can reduce the effect from coil misalignment [2], have been carried out. It is also important to design the magnetic cores for WPT for improvement of the efficiency of WPT systems. The topology optimization has been shown effective for this purpose owing to its high flexibility in shape representation [3]. The safety of WPT devices has to be also carefully considered in its development. The limitation of magnetic flux exposure to human bodies in frequency band ranging from 3 kHz to 10MHz is stipulated as 27 μT by ICNIRP [4]. To consider both safety and efficiency, the multi-objective topology optimization of a WPT device with respect to the efficiency and leakage flux density has been shown effectively [5].

In this work, we pay attention to the potential risk caused by foreign objects which threats safety of WPT systems. There are two kinds of foreign objects which are usually concerned: living objects and foreign metal objects [6]. The risk from living objects is somehow similar to what is described above; the magnetic flux exposure to creature's body is dangerous. While the latter, relevant to metal objects, can cause dangerous electric discharge and fire accidents due to the localized strong electric field around metal edges and also eddy currents, as schematically shown in Figure. 1.

For this reason, it is necessary to develop foreign object detection (FOD), including living object detection (LOD) and metal object detection (MOD). Many studies to realize FOD in WPT system has been reported. Typically, additional thermal cameras for LOD and MOD [7], and detection coils for MOD [8] have been introduced for FOD to improve the accuracy and effectiveness in both LOD and MOD. However, these additional devices would bring extra cost and complexity to WPT systems. For this reason, sensorless FOD is desirable for relatively lower cost and complexity.

In this paper, a simple detection method of foreign metallic objects without additional sensors and equipment is proposed. In this method, the existence of foreign metal object is identified from the change in the locus of the input impedance. Because the impedance locus has highly complicated changes owing to the metal object and misalignment in the coils, we adopt here the machine learning to distinguish the impedance loci. In particular, we use neural network (NN), support vector machine (SVM) and naïve Bayes classifier (NBC), which are trained to give correct identification for various impedance loci with and without metallic object that can have different size and location and with different coil alignment conditions. The impedance loci for the training are computed using finite element method (FEM) by software JMAG®. The experimental verifications using aluminum cylinder, empty aluminum can and steel key as foreign metal objects are also carried out and compared with the numerical results. The novelty and universality of this work lines in the fact that the machine learning is introduced for detection of abnormality, and its feasibility is tested using EM simulation as well as experiments.

It is remarked that the authors presented the basic idea and results of the proposed method at IGTE Symposium 2020 on 22th September 2020. Until this date, so far as the authors know, there had been no studies for application of machine learning to sensorless FOD. Afterward, a sensorless FOD for WPT based on neural network in megahertz frequency band was proposed in [9].

II. EQUIVALENT CIRCUIT

In this work, resonance WPT is considered whose coil system is illustrated in Fig.2. An assumed foreign metal object is included in Fig.2(b). The input impedance and

inductance (L_1, L_2) are computed using FEM by JMAG®, while the two coils are simply modeled as a lump whose skin effect is not considered during simulation. The shape parameters are listed in TABLE I.

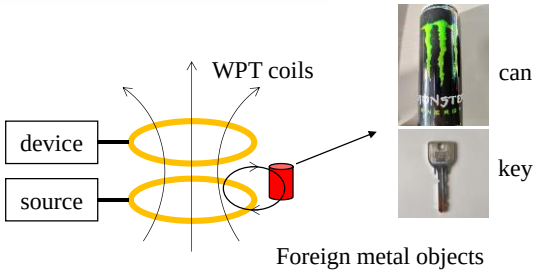

Figure 1: Risk caused by foreign metallic object in WPT system.

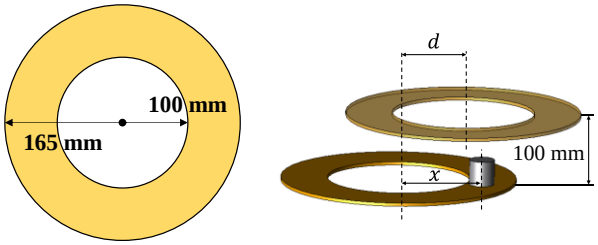

(a) coil (b) Extremal position

Figure 2: Model of WPT coil and foreign metal object

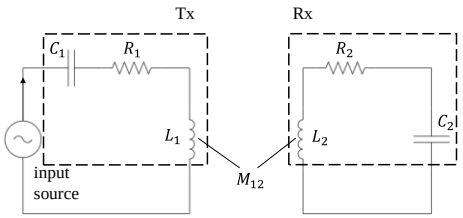

(a) Equivalent circuit

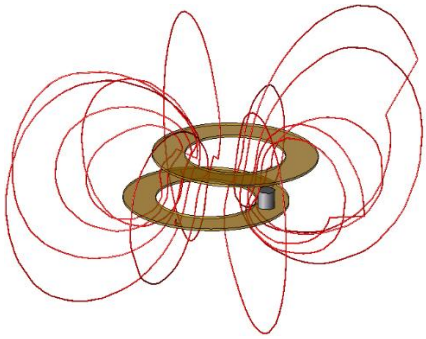

(b) Magnetic flux distribution

Figure 3: Equivalent circuit and magnetic flux distribution around the WPT coils with misalignment and foreign metal object.

TABLE I
SHAPE PARAMETERS

Inner radius of coil	100 mm
Outer radius of coil	165 mm
Turns of coil	16
Transmission distance	100 mm
Coil misalignment	0 ~ 160 mm
Metal object offset	0, 130, 200 mm
Diameter and height of aluminum cylinder	35 mm

TABLE II
PARAMETERS OF CIRCUIT.

Input source (current)	I_{rms} = 20 mA
R_1, R_2	1 Ω
C_1, C_2	45 nF

The equivalent circuit for the WPT system shown in Fig.2 is illustrated in Fig.3(a), where the primary and secondary coils are modeled as the series RLC resonance circuits. In the FE analysis, the currents are computed from the circuit shown in Fig.3(a). Moreover, the coil is modeled as a pancake without discretizing into the wires assuming that the wire radius is sufficiently smaller than the skin depth.

The circuit parameters are listed in TABLE I. The values of capacitor (C_1, C_2) in both sides are set identical, making the circuit to achieve resonance at about 81 kHz. R_1 and R_2 are the inner resistance of coils. Although the mutual inductance M_{12} between transmitting (Tx) and receiving (Rx) coils is included in the equivalent circuit, those among Tx, Rx and metal object are not included. For simplicity, the load of Rx is assumed as 0 in simulation and experiments validations. The effect of load will be discussed in IV.C.

The influence of the metal object on the input impedance is evaluated by FEM. A typical magnetic field distribution is shown in Fig. 3(b), where the eddy currents in the metal object is considered.

III. PROPOSED METHOD BASED ON MACHINE LEARNING

A. *Data preparation*

Considering both effects coming from the metal object and coil misalignment, in the simulations, the displacement of the secondary coil d is varied from 0 mm to 160 mm, and the position x of the metal object measured from the center of the primary coil is set to 0 mm, 130 mm and 200 mm. As for the foreign metal object, we assume an aluminum cylinder of height 35 mm and diameter 35 mm.

In total, 116 cases are simulated, where the metal object is considered in 65 cases while it is not included in other cases.

In each case, the input resistance R_i and reactance X_i at frequencies ranging from 75 kHz to 85 kHz are computed at intervals of 500Hz to obtain the 11 sampling data. This results in a vector $\boldsymbol{Z} = [R_1, \dots, R_{11}, X_1, \dots, X_{11}]^t \in \mathbb{R}^{22}$. Those values are connected to obtain a locus of the input impedance on an $R - X$ plane for each case. We construct $\boldsymbol{Z}$ with labels of 0 or 1 representing without or with metal object. All the impedance vectors are randomly assigned into 2 datasets and treated as the training and validation data. The three machine learning methods described below, which are widely used for classification problems, are trained to give correct judgement to the labels of data vectors.

B. *Neural network*

A simple neural network (NN) realized by Tensorflow® [10] in Python is used in this work. The hyper parameters for training of NN are listed in TABLE III. The hyper parameters are determined by trial-by-error while it needs small computing cost compared to the field

computations.

The loss function for NN based on the sparse categorical cross entropy is used, where $\hat{y}_i$ is the i-th scalar value in the model output, y_i is the corresponding target value, and n is the number of scalar values in the model output.

$$\text{Loss} = -\sum_{i=1}^{n} y_i \cdot \log \hat{y}_i \qquad (1)$$

Four layers which are composed of 64, 32, 16, 2 neurons, respectively, are configured, as shown in Fig .4. ReLU is set after the dense layers as activation functions. The data vectors of the input impedances are input to NN after normalization, while {0,1} representing the existence probability of the metal object is output.

TABLE III
HYPER PARAMETERS OF NEURAL NETWORK

Batch size	5
Epochs	500
Activation function	ReLU
Optimizer	Adam [11]
Learning rate	0.001
Loss function	Sparse categorical cross entropy

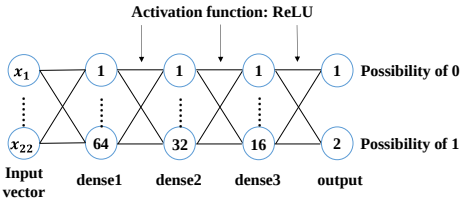

Figure 4: Structure of NN

C. *Support vector machine*

Support vector machine (SVM) is a supervised learning method used for classification and regression [12]. The idea of SVM is to find a $(p-1)$-dimensional hyperplane which separates the p-dimensional vectors into different classes with widest gaps. When facing non-linear classification, a kernel function is introduced to implicitly map the data into high-dimensional feature spaces, where the classification can be turned into linear.

In this work, we adopt the radial basis function kernel (RBF kernel) defined by

$$K(\boldsymbol{x}, \boldsymbol{x}') = \exp(-\gamma \|\boldsymbol{x} - \boldsymbol{x}'\|^2) \qquad (2)$$

for SVM, where $\boldsymbol{x}$ and $\boldsymbol{x}'$ represent the feature vectors in the input space. The classification based on SVM is implemented by scikit-learn® [13] in Python, in which we assume that $\gamma = 1/\sigma^2$ for simplicity where σ^2 denotes the valiance of the data. These values are summarized in TABLE IV.

TABLE IV
VALUE OF $\gamma^2 = 1/\sigma^2$

Simulation, no load	0.0442
Simulation, 20Ω load	0.0439
Experiment, cylinder	0.0449
Experiment, can	0.0490
Experiment, key	0.0477

D. *Naive Bayes classifier*

Naive Bayes classifier (NBC) is a simple probabilistic classifier based on Bayes' theorem, which is expressed as

$$P(C|\boldsymbol{Z}) = \frac{p(\boldsymbol{Z}|C)P(C)}{p(\boldsymbol{Z})} \qquad (3)$$

where C is $\{0, 1\}$ that represents existence of a metal object, $\boldsymbol{Z}$ is the input impedance locus. The prior probability $P(C)$ and likelihood $p(\boldsymbol{Z}|C)$ are determined from the training data while $p(\boldsymbol{Z})$ is assumed to be uniform distribution. The classification based on NBC is implemented by scikit-learn ® in Python as well.

IV. SIMULATION RESULTS

A. *Loci of input impedances*

The loci of the input impedance for 116 simulated cases are shown in Fig. 5, where blue and orange loci denote the cases without and with a metal object, respectively.

When the coil misalignment d increases, the largest input resistance in frequency range decreases, and the whole locus tends to shrink. The locus also tends to shrink owing to the existence of a metal object as shown in Fig.5.

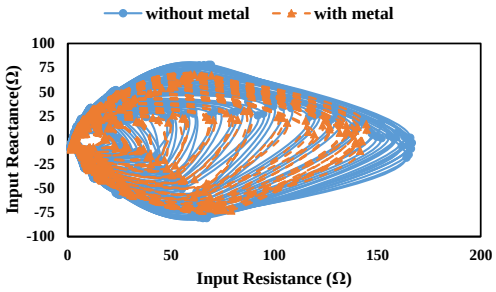

Figure 5: Loci of input impedances from simulations (no load).

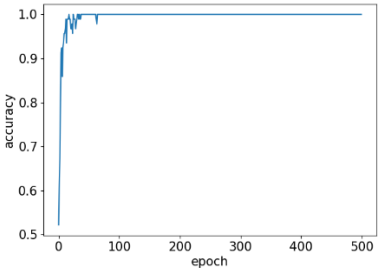

(a) Accuracy for training dataset

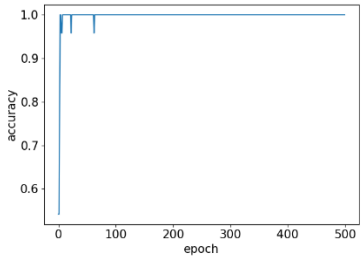

(b) Accuracy for validation dataset

Figure 6: Training history of NN (simulations).

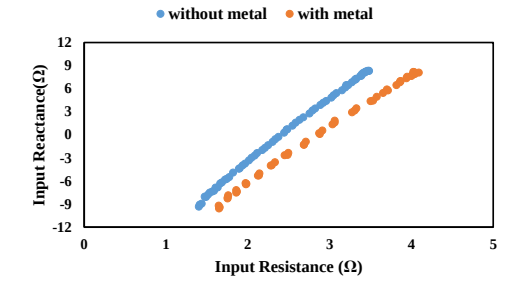

(a) At 75 kHz

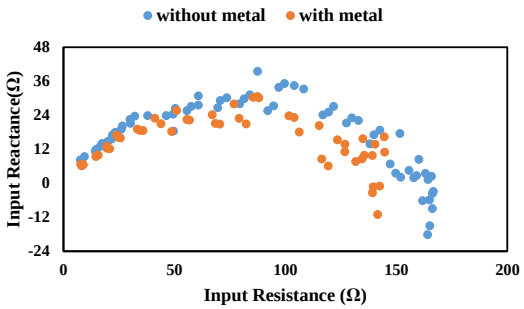

(b) At 81 kHz

Figure 7: Input impedance points. (no load)

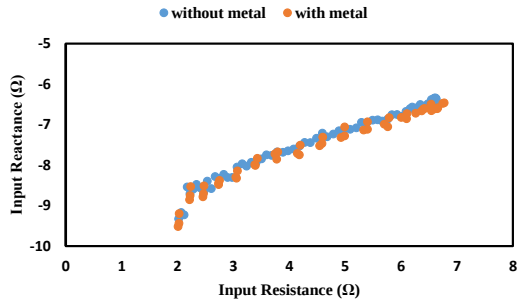

(a) At 75 kHz

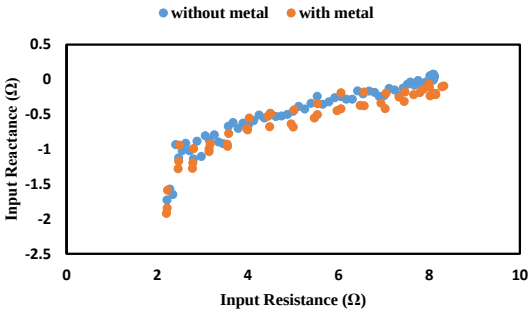

(b) At 81 kHz

Figure 8: Input impedances points (20Ω load).

B. *Training results*

The 80% of the whole training data, that are 116 loci of the computed input impedance, are used as the training data while the others are used as the validation set. The training histories of NN for the training and validation datasets are shown in Fig.6, and the performance of the three machine learning methods after training are summarized in TABLE V.

As shown in TABLE V, all of the three machine learning methods have accuracy better than 85%. In particular, NN has no classification errors with fast convergence.

To know the reason why all the methods get high accuracy, the input impedance values at 71 kHz and also 81 kHz that is near the resonance frequency are plotted in Fig.7, respectively. It can be seen that there are clear differences between the cases with metal and without metal especially at 71 kHz, which is considered to be the key of the successful classification.

TABLE V
ACCURACY OF THREE MEHODS FOR VALIDATION DATA (SIMULATIONS, NO LOAD)

NN	100%
SVM	96%
NBC	88%

C. *Effect of load*

Above mentioned results are obtained assuming no load on Rx. To consider if the load affects the classification accuracy, we connected the load, 20Ω, to Rx. The resultant input impedance points at 75 and 81 kHz are shown in Fig.8. In this case we find no clear differences between the input impedance values with and without metal, in contrast to the results shown in Fig. 7. This is understood from the fact that the quality factor is reduced when the load is connected to Rx. The average accuracy for five-fold cross validation is summarized in TABLE VI. It can be seen that the accuracy reduces by about 20% owing to the load on Rx, which indicates that the addition of load will make classification harder. For this reason, we conclude that the proposed method should be used under the condition that Rx is short.

TABLE VI
ACCURACY OF THREE METHODS FOR VALIDATION DATA (SIMULATIONS, LOAD = 20Ω)

NN	77.6%
SVM	73.2%
NBC	63.8%

V. EXPERIMENTAL RESULTS

We perform experimental verification where the input impedance is measured. The LCR meter and coils used in experiments are shown in Fig.9. The shape parameters of coils and circuit parameters are set to the same as those in the aforementioned simulation-based method.

There are three foreign metal objects used in experiments, which are shown in Fig.10. The aluminum cylinder has been considered in the simulation-based method while the empty aluminum can has a diameter of 55 mm and height of 155 mm, and the length of the steel key is 60 mm.

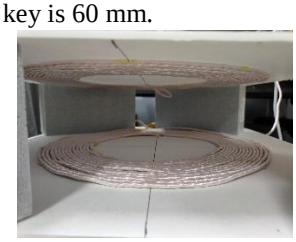

(a) coils

(b) LCR meter (HIOKI IM3536)

Figure 9: Experimental devices

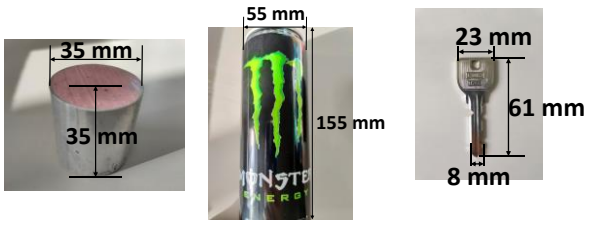

(a) Cylinder (b) Can (c) Key

Figure 10: foreign metal objects used in experiments.

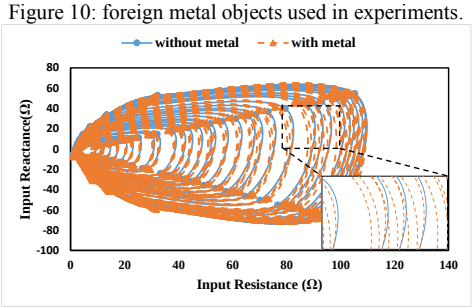

Figure 11: Loci of input impedances from experiments (cylinder).

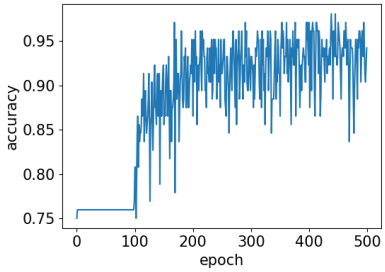

(a) Accuracy for training dataset

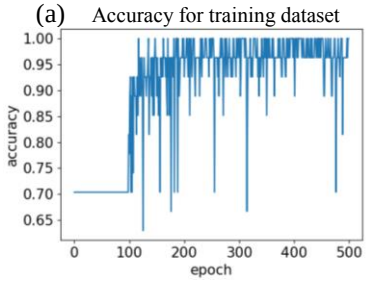

(b) Accuracy for validation dataset

Figure 12: Training history of NN (experiments, cylinder).

A. *Aluminum cylinder*

In the experiment, the aluminum cylinder is placed 0 mm, 130 mm and 200 mm away from the center of Tx coil, which is set to the same as the simulations. The input impedance values for 131 cases have been measured here, where 33 cases are without metal and 98 cases are with metal.

The input impedance loci of the 131 cases are shown in Fig.11. The tendencies in the loci obtained from the simulation and experiments seem similar although there are quantitative differences between them which are possibly caused by factors such as skin effect and noise of devices. The differences in the loci for the cases with and without metal object are unclear though NN still obtains good performance as described below. The training history of NN is shown in Fig.12, and the performances of the three methods are listed in TABLE VII.

Although the accuracy for training and validation data has fluctuations in the history, both of them finally reach over 90%. In contrast to NN, the accuracy of SVM and NBC deteriorates compared to the simulation-based classification.

TABLE VII
ACCURACY OF 3 METHODS FOR VALIDATION DATA (EXPERIMENTS, CYLINDER)

NN	96% ~ 100%
SVM	70%
NBC	58%

B. *Empty aluminum can*

When using the empty aluminum can as the foreign metal object, the input impedance loci show obvious differences between cases without and with metal as shown in Fig.13, where 101 cases are measured, including 33 and 68 cases without and with metal. The can is laid in experiments, and placed in the center of Tx coil, or 100 mm far away from the central axis.

It seems easier for NN to make correct judgement for the cases. As shown in Fig.14, during the training, NN quickly reaches at accuracy of 100% for both training and validation data. In TABLE VIII, it can be seen that all the three machine learning methods have accuracy over 90%. These results come from the clear difference in the loci shown in Fig.13. However, it would be difficult for us to pick the features from the loci for classification. The machine learning methods automatically take those features from the data.

TABLE VIII
ACCURACY OF 3 METHODS FOR VALIDATION DATA (EXPERIMENTS, CAN)

NN	100%
SVM	100%
NBC	90%

C. *Steel Key*

In the experiments with key, the positions of the key are set to the same as the cylinder cases. In total, 136 cases are measured, including 34 without metal and 102 with metal.

The input impedance loci of all the cases are shown in Fig.15. It seems hard to find the differences between the loci without and with metal. As a result, as shown in Fig. 16 and TABLE IX, the accuracy of NN remains unchanged during the training, and all the three machine learning methods judge all the cases in validation as with metal, so the accuracy of them are all 71%, which is exactly the proportion of cases with metal in the validation dataset.

TABLE IX
ACCURACY OF 3 METHODS FOR VALIDATION DATA (EXPERIMENTS, KEY)

NN	71%
SVM	71%
NBC	71%

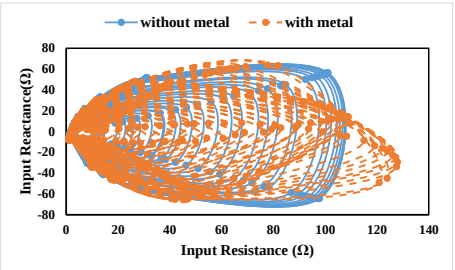

Figure 13: Loci of input impedances from experiments (can).

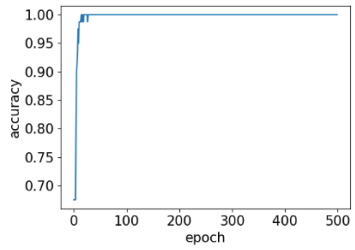

(a) Accuracy for training dataset

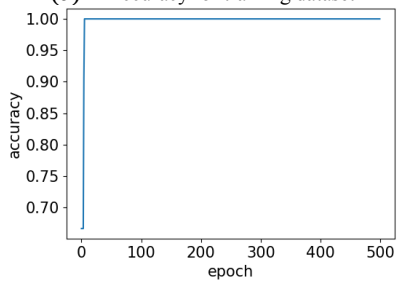

(b) Accuracy for validation dataset

Figure 14: Training history of NN (experiments, can).

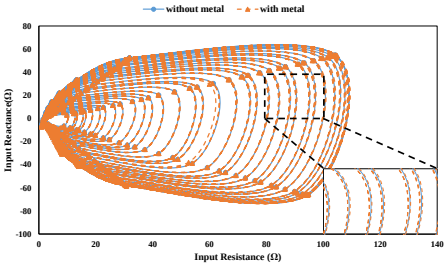

Figure 15: Loci of input impedances from experiments (key).

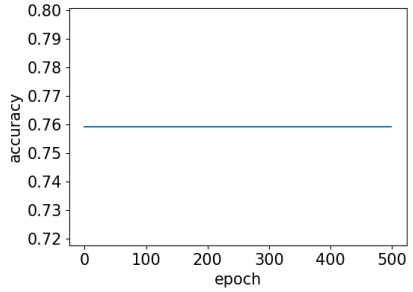

(a) Accuracy for training dataset

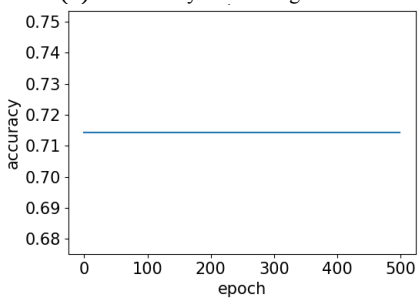

(b) Accuracy for validation dataset

Figure 16: Training history of NN (experiments, key).

The input impedance loci of all the cases are shown in Fig.15. It seems hard to find the differences between the loci without and with metal. As a result, as shown in Fig. 16 and TABLE IX, the accuracy of NN remains unchanged during the training, and all the three machine learning methods judge all the cases in validation as with metal, so the accuracy of them are all 71%, which is exactly the proportion of cases with metal in the validation dataset.

It is concluded that the influence from the key to the input impedances is so small that the methods cannot make correct classification at all.

VI. CONCLUSION

In this paper, a new detection method of a foreign metal object without additional sensors or coils using machine learning has been proposed. The input impedances of a WPT system with and without the metal object having different misalignment distances are obtained by FEM and experiments, and are used as the training data for machine learning. When relatively large objects such as an aluminum cylinder and empty can are set as the foreign metal object, the accuracy of this method is satisfactory. In particular, NN gives the best performance for them. When the metal object is small, as in the case for the key, the proposed method does not work well. Moreover, the proposed method should be used under the condition that the receiving circuit is short because its accuracy becomes worse when the load is introduced to Rx. These shows the limitation of the method. In future, we will study the quantitative limitation in the size for the successful detection. Moreover, we will develop a method to improve the classification accuracy for the load cases.

REFERENCES

[1] X. Liu, S. Y. Hui, "Optimal design of a hybrid winding structure for planar contactless battery charging platform," *IEEE Trans. Power Electronics*, vol. 23, no. 1, pp. 455-463, 2008.

[2] M. Budhia, et al. "Development of a single-sided flux magnetic coupler for electric vehicle IPT charging systems." *IEEE Transactions on Industrial Electronics*, vol. 60, no. 1, pp. 318-328, 2013.

[3] Y. Otomo, H. Igarashi, "A 3-D Topology Optimization of Magnetic Cores for Wireless Power Transfer Device," *IEEE Trans. Magn*., vol. 55, no. 6, pp.1-5, 2019.

[4] International Commission on Non-Ionizing Radiation Protection, "Guidelines for limiting exposure to time-varying electric and magnetic fields (1 Hz to 100 kHz)," *Health Phys.*, vol. 99, no. 6, pp. 818–836, 2010.

[5] Y. Gong, Y. Otomo, H. Igarashi, "Multi-objective topology optimization of magnetic couplers for wireless power transfer." *International Journal of Applied Electromagnetics and Mechanics,* Preprint, pp. 1-9, 2020.

[6] Y. Zhang, Z. Yan, J. Zhu, et al, "A review of foreign object detection (FOD) for inductive power transfer systems", *eTransportation*, vol. 1, 10002, 2019.

[7] T. Sonnenberg, et al. "Combined foreign object detection and live object protection in wireless power transfer systems via real-time thermal camera analysis." *2019 IEEE Applied Power Electronics Conference and Exposition (APEC)*. IEEE, 2019.

[8] L. Xiang, et al. "Foreign object detection in a wireless power transfer system using symmetrical coil sets." *IEEE Access,* vol. 7, no. 7, pp. 44622 - 44631, 2019.

[9] M. Ote, et al. "Foreign Object Detection for Wireless Power Transfer Based on Machine Learning." *2020 IEEE Wireless Power Transfer Conference (WPTC)*. IEEE, 2020.

[10] M. Abadi, et al, "Tensorflow: Large-scale machine learning on heterogeneous distributed systems", arXiv preprint arXiv:1603.04467, 2016.

[11] DP. Kingma, J. Ba. "Adam: A method for stochastic optimization." *arXiv preprint arXiv*:1412.6980 (2014).

[12] C. Cortes, V. Vapnik, "Support-vector networks". Machine learning, 1995, 20(3): 273-297.

[13] F. Pedregosa, et al. "Scikit-learn: Machine learning in Python." *the Journal of machine Learning research 12*: 2825-2830, 2011.